

ScienceDirect



IFAC PapersOnLine 55-27 (2022) 293-298

Adaptive Discrete Mapping of Dynamic Nanomechanical Property of Soft Materials on Atomic Force Microscope *

Jingren Wang,* Qingze Zou,** Senli Guo***

- * Department of Mechanical & Aerospace Engineering, Rutgers, the State University of New Jersey, Piscataway, NJ 08854 USA (email: jw986@scarletmail.rutgers.edu)
- ** Department of Mechanical & Aerospace Engineering, Rutgers, the State University of New Jersey, Piscataway, NJ 08854 USA (email: qzzou@soe.rutgers.edu)
- *** Bruker Nano Surfaces & Metrology, 112 Robin Hill Road, Santa Barbara, CA 93117 (e-mail:senli.guo@bruker.com)

Abstract: In this paper, an adaptive discrete nanomechanical mapping (A-DNM) technique is proposed for mapping time-varying nanomechanical properties of soft sample using atomic force microscope (AFM). Mapping time-varying nanomechanical properties is needed to investigate samples undergoing dynamic evolutions. However, current continuously-scanning-based approach is too slow to capture the time-elapsing variations over the entire sampled area, or is limited to small-area mapping only. Contrarily, we propose to extend a discrete nanomechanical mapping scheme where only a set of discrete locations (points of interests, POIs) are visited, by adaptively adjust the distribution of the measurement time between the POIs through a batch process. The proposed approach is demonstrated by implementing it to map the nanomechanical evolution of a poly(3-hydroxybutyrate-co-3-hydroxyvalerate) (PHBV) polymer during the crystallization process.

Copyright © 2022 The Authors. This is an open access article under the CC BY-NC-ND license (https://creativecommons.org/licenses/by-nc-nd/4.0/)

1. INTRODUCTION

In this paper, an adaptive discrete nanomechanical mapping (A-DNM) technique is proposed to use atomic force microscope (AFM) to measure spatial-temporal nanomechanical evolutions of samples undergoing dynamic evolutions, such as the crack propagation of glassy polymers George et al. (2018). In these nanoscale dynamic processes, capturing the time-elapsing properties of the species is of utmost interests and importance, for example, to study the crystallization process of polymer insitu Hobbs et al. (2009). The existing continuous-scanningbased AFM technologies (Pittenger et al., 2013), however, are incapable of achieving such a measurement requirement, as these technologies are limited to capturing nanoscale dynamics in a small area Kodera et al. (2021), or are too slow to reveal dynamic evolutions occurring in a few minutes or faster when the measurement area increases. Built upon a recently-developed discrete nanomechanical mapping (DNM) approach Wang et al. (2020), this work aims to tackle these challenges through the development of an adaptive discrete nanomechanical mapping technique.

Limitations exist in current continuous-scanning-based AFM technologies for mapping fast dynamic phenomena at nanoscale. The mapping speed of AFM can be increased by improving the working bandwidth of the cantilever actuation and positioning system through hard-

ware advances, software (control algorithms) innovations, or combination of both. For example, by using highspeed piezoelectric actuators and cantilever, sub-cellular dynamic evolutions (e.g., motor proteins) have been captured over a small sample area (a couple of μm^2 or smaller) Kodera et al. (2021), but not for sample area of larger size. Alternatively, the mapping speed over a large sample area can be improved through the development of control algorithms to better compensate for the adverse effects of the piezo-cantilever actuation system Ren et al. (2014). Although the mapping (imaging) speed can be dramatically increased (e.g., over twenty times) Ren et al. (2014), the scanning speed is still too slow to discern dynamic evolutions of the sample occurring in a few minutes or faster. Fast dynamic evolutions at one location can be monitored through repetitive measurements Yan et al. (2017). However, this one-point measurement does not provide a global view over the sample. Thus, techniques need to be developed for mapping nanoscale dynamic phenomena using AFM.

The recently-developed rapid discrete nanomechanical mapping (R-DNM) Wang et al. (2020) is promising to overcome the limitations in the existing continuous-scanning approach. Instead of scanning the entire sampled area, the R-DNM is to measure nanomechanical properties only at a set of chosen locations (i.e., points of interests (POIs)) over the sampled area, thereby, dramatically reducing the mapping time while the POIs can be selected to represent the global evolution. Such a notion of discrete mapping has also been explored in topography

 $[\]star$ Support from NSF Grants IIBR-1952823 and CMMI-1851907 are gratefully acknowledged.

imaging Braker et al. (2018). However, the increase of mapping/imaging speed obtained is limited by the time consumed by the cantilever probe engagement and withdrawal in each discrete piecewise imaging Braker et al. (2018). Rapid probe engagement and withdrawal is complicated by the stiff nonlinear dynamics of probe-sample interaction during the engagement and withdrawal process. Such a challenging nonlinear tracking and positioning problem is addressed through a learning-based online optimization approach Wang and Zou (2020), central to the effectiveness of the R-DNM technique, as has been demonstrated in AFM experiments on polymers Wang et al. (2020). The R-DNM also offers additional flexibility to tailor the mapping sequence to accommodate the sample, for example, to distribute the POIs based on the heterogeneity of the sample, or to adjust the distribution of the measurement time between the POIs for samples undergoing nonuniform dynamic evolution. This adaptive mapping idea is explored in this paper.

The main contribution of this article is the development of an A-NDM technique for samples undergoing rapid dynamic mechanical evolution. Built upon the R-NDM method, the A-NDM technique addresses two challenges arising from the dynamic mechanical variations. First, the time-varying probe-sample contact occurring during dynamic mechanical evolution is accounted for by estimating the sample height at each POI in real-time, and using it to adjust the probe transition between two successive POIs. Secondly, an online adaptive mapping sequence planning is developed to online adjust the distribution of the measurement time between the POIs to capture the spatial-temporal distribution of the sample. Furthermore, the rapid engagement, withdrawal and transition of the probe in the discrete mapping process are also enhanced for better mapping efficiency. The proposed approach is illustrated through AFM experiment on mapping the nanomechanical evolution of a PHBV sample undergoing the crystallization process.

2. NANOMECHANICAL MAPPING OF SOFT MATERIALS UNDER DYNAMIC EVOLUTION: PROBLEM FORMULATION

2.1 Adaptive rapid discrete nanomechanical mapping

Built upon the DNM framework, the proposed adaptive DNM (A-DNM) constitutes three steps as follows:

Step 0: Initialization: Measure the initial sample information (e.g., height and relative stiffness) at the chosen POIs. and determine an initial mapping sequence.

Step 1: For a given mapping sequence, measure the nanomechanical properties at all the sampling locations via the following steps:

Step 1.1: At any given POI, rapidly engage the probe to the sample with the desired force load, during the engagement accounting for the time-varying sample-topography contact variation (see figure 1 (a)).

Step 1.2: At that POI, rapidly measure the nanomechanical property of the sample in the desired frequency spectrum Wang et al. (2020) (see figure 1 (b)).

Step 1.3: Rapidly withdraw the probe from the sample Wang and Zou (2020) without inducing large cantilever vibrations and/or sample deformation (see figure 1 (c));

Step 1.4: Rapidly and precisely transit the probe to the next POI both laterally and vertically to reposition the probe to reach to the same initial position at the next POI (see figure 1 (d)), then repeat the above Steps 1.1 to 1.4 until all the POIs have been covered;

Step 2: Adaptively online plan the mapping sequence in the next round of measurement (see figure 1 (e));

Step 3: Repeat the above Step 1 and Step 2 until the total measurement is accomplished.

The above Steps 0 to 3 extends those in the DNM technique Wang et al. (2020). Particularly, Steps 1.2 to 1.4 are the same as those described previously and the readers are referred to Ref. Wang et al. (2020) for the detail. The proposed A-DNM technique aims to address two objectives:

- \mathcal{O}_1 : Account for the time-varying sample-topography contact variation and optimize the probe engagement and transition processes to improve the online effi-
- \mathcal{O}_2 : Online adaptively plan the nanomechanical mapping sequence to accommodate the dynamic evolutions at the POIs.

2.2 \mathcal{O}_1 : Optimal Probe Engagement and Transition under Time-Varying Sample Topography Variation

We start with estimating the sample topography variation in real-time.

Online Sample Topography Estimation in Real-time An iterative approach is proposed to estimate the sample topography at each POI. As the nanomechanical measurement at a POI is acquired repetitively in loops (see Sec. 2.1), past measurements of the probe-sample interaction can be utilized to predict the sample height in current measurement. Thus, we consider the estimation of the sample height at any given k^{th} POI in the i^{th} round of mapping, \hat{z}_k^i , by using the probe-sample interaction force measured during the $(i-1)^{th}$ probe engagement, i.e., the preload force, $F_{pre,k}^{i-1}$. Particularly, during the probe en gagement process, the probe is first engaged to the sample as if there were no time-varying topography variationthe probe is first driven to engage to the sample under the same control input profile (see Wang and Zou (2020)) towards the desired value $\mathbf{F}_{\mathrm{set}}$, then the deviation of the preload force, $\mathbf{F}_{\mathrm{set}} - F_{pre,k}^{i-1}$, if large, will be compensated for via a feedforward-feedback control (described below). Thus, this deviation of the preload force is directly proportional to the change of the sample height (at the k^{th} POI) between the $(i-1)^{th}$ and the i^{th} round of mapping. Thus, for any i > 1,

$$\hat{z}_k^i = \begin{cases} \alpha \hat{z}_k^{i-1} + (1-\alpha)z_k^{i-1} & \text{if } \left| \mathbf{F}_{\text{set}} - F_k^{i-1} \right| < \epsilon_F; \\ \hat{z}_k^{i-1} + \beta z_{k,eng}^{i-1}, & \text{Otherwise;} \end{cases}$$
where, respect to the $(i-1)^{th}$ round of mapping, \hat{z}_k^{i-1}

is the estimated sample height at the k^{th} POI, z_k^{i-1} is the

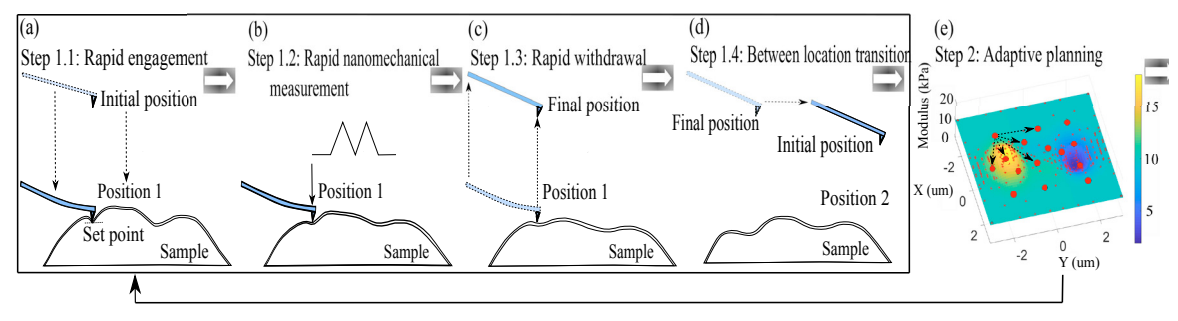


Fig. 1. Schematic illustration of ADNM with steps of (a) rapid probe engagement, (b) rapid nanomechanical measurement, (c) rapid probe withdrawal, (d) adaptive planning, and (e) between location probe transition of the ADNM process.

probe position corresponding to the preload force, ϵ_F is the chosen threshold value, $z_{k,eng}^{i-1}$ is the amount of additional probe displacement during the engagement, and α , β are the weighting coefficients and ϵ_f is the threshold value, respectively. Initially, z_k^0 is set as the sample height value obtained through an initial measurement process of the sample height at all POIs, same as in the DNM approach (see Wang and Zou (2020) for the detail).

Optimal Rapid Probe Transition and Engagement under Time-varying Sample Topography Change Next, the above estimated sample topography is used to compensate for the time-varying effect on the probe transition and engagement processes.

Probe Transition Under Time-Varying Sample Height Change Due to the time-varying sample topography, the desired vertical transition distance of the probe (called the vertical-transition distance) from one POI to the next will be different. Thus, for the engagement at the k^{th} POI in the i^{th} round of mapping, the vertical transition distance at the $(k+1)^{th}$ POI, $\hat{z}^i_{k+1,tran}$, is estimated as

 $\hat{z}_{k+1,tran}^i = z_{tran}^* + \hat{z}_k^i + z_{k,wdr}^{i-1}, \quad i \geq 1 \tag{2}$ where, respectively, z_{tran}^* is the nominal vertical transition distance, \hat{z}_k^i is the estimated sample height obtained above, and $z_{k,wdr}^{i-1}$ is the vertical withdrawal distance after the previous $(i-1)^{th}$ measurement (i.e., after the withdrawal). The nominal vertical distance z_{tran}^* is the distance between the average sample surface height and the initial position of the probe for the engagement (the same initial probe position is maintained at each POI such that the same rapid engagement control input can be applied with only minor changes, described below immediately), where the average sample surface height is measured during the initialization step (Step 0) of the mapping process as in the DNM method Wang and Zou (2020). This quantification of the vertical transition distance reflects the fact that the timevarying sample height change \hat{z}_k^i is only a small fraction of the nominal value z_{tran}^* . As such, the corresponding control input is also close to the nominal one—the control input for the nominal transition of the probe between POIs, $u^*_{tran}(\cdot)$. In particular, $u^*_{tran}(\cdot)$ is obtained a priori during the initialization step, by first designing the desired transition trajectory using the optimal output transition technique Wang and Zou (2020) (with the output boundary condition given by z_{tran}^*), and secondly, tracking the desired trajectory using iterative learning control such as the MIIC technique Kim and Zou (2013), as presented in Wang et al. (2020). This proximity of input implies that the control input for transiting the probe from the k^{th} to the $(k+1)^{th}$ POI in the i^{th} mapping, $u^i_{k,tran}(\cdot)$, can be obtained from the nominal one $u^*_{tran}(\cdot)$ via scaling as

$$u_{k,tran}^{i}(t) = \frac{z_{k,tran}^{i}/K_{DC}}{U_{tran}^{*}} u_{tran}^{*}(t)$$
 for $t \in [0, T_{ztran}]$

where K_{DC} is the DC-Gain of the z-axis piezoelectric actuator, and $U_{tran}^* = \|u^*tran(\cdot)\|_{\infty}$ is the amplitude of the initial engagement control input, respectively.

This input-scaling idea is also utilized to achieve high-efficient lateral transition of the probe between POIs: First, an optimal control input for the lateral between-POI transition is obtained in the same manner as above Wang et al. (2020), and applied to the feedback control loop of the lateral piezo actuator (the feedback control is employed to remove the creep and drift effect of the piezo during the measurement when then piezo is hold at the POI). Secondly, the lateral control input is obtained by scaling this normal lateral transition input as in Eq. (3).

Rapid Probe Engagement Under Time-Varying Sample Height Change The effect of time-varying sample height is further accounted for during the probe engagement process. The proposed engagement process is built upon and extends the learning-based partition and sequential optimization approach developed in the DNM technique Wang and Zou (2020): The engagement process is partitioned into three different phases (according to the probe-sample distance and the characteristics of the probesample interaction force), and the corresponding control input in each phase is designed and optimized accordingly. The first two phases (see Fig. 1 in Wang and Zou (2020)), called the pre-contact and the initial-engagement phase, respectively, are characterized by the probe from being far away to being in a close proximity of the sample surface, and from that to being in contact with the sample with a small probe-sample contact force, respectively. We propose to compensate for the sample topography changes in the third phase (called the final-engagement phase) during which the probe is driven from the initial sample contact position to engage with the sample at the desired preload force.

Specifically, a feedforward-feedback switching control is proposed to achieve rapid robust engagement with high-efficiency. First, during the Initialization Step (Step 0), the rapid engagement technique in Wang and Zou (2020)

is applied to a POI (e.g., the first POI), and a nominal control input for the three phases above are obtained. Then in each i^{th} round of mapping, at any given k^{th} POI, this nominal control input is applied as a feedforward control to drive the probe from the end-of-transition probe position to engage to the sample with the contact force around the setpoint of the preload level. Next, to account for the uncertainty and variation caused by residual sample height variation effect and disturbance, the feedforward control is switched to a PI-feedback controller. Care is taken to maintain a smooth transition at the switching instant (by smoothly transiting the setpoint value from the measured force value to the desired preload force).

2.3 \mathcal{O}_2 : Adaptive Planning of Mapping Sequence for Dynamic Heterogenous Sample

Next, we present the proposed adaptive planning scheme for mapping dynamic heterogenous sample.

Online estimation of relative nanomechanical dynamics between POIs We propose a POI-dynamics index based on the cantilever deflection measurement to quantify the relative nanomechanical dynamics between POIs. In the proposed A-DNM approach, the nanomechanical measurement at each POI is measured under the same initial probe-sample contact and the same excitation input (applied to the piezoelectric actuator). Thus, the amplitude of the cantilever deflection—proportional to the probesample interaction force—directly represents the stiffness of the sample. At any given k^{th} POI, the averaged cantilever deflection in the i^{th} measurement period $\bar{d}_k[i]$ below obtained is used.

$$\bar{d}_{k}[i] = \frac{1}{N_{meas}} \sum_{j=0}^{N_{meas}} \left| d_{k}^{i}(j) - \hat{d}_{k,dft}^{i}(j) - d_{k}^{i}(0) \right|, \quad (4)$$

where, respectively, $d_k^i(j)$ is the j^{th} sampled measurement of the cantilever deflection during the i^{th} measurement at the k^{th} POI, with N_{meas} the total number of samples taken in one measurement period, $d_k^i(0)$ is the corresponding initial measurement, and $\hat{d}_{k,dft}^i(j)$ is the estimated deflection deviation due to the drift of the piezoelectric actuator during the measurement.

Using the average cantilever deflection $d_k[i]$, the POI-dynamics index is to characterize the mechanical fluctuation at each POI between two successive round of mappings. Specifically, the first- and the second- order time-variation of $\bar{d}_k[i]$, i.e., the speed and the acceleration of $\bar{d}_k[i]$, are considered: The POI-dynamics index for the k^{th} POI, $\phi_{k,Dyn}[\cdot]$, is given by

$$\phi_{k,Dyn}[i] = \lambda |\bar{v}_k[i]| + (1 - \lambda) |\bar{a}_k[i]|, \qquad (5)$$

where, respectively, $\lambda \in (0, 1)$ is the weight, and $\bar{v}_k[i]$ and $\bar{a}_k[i]$ are the averaged velocity and the averaged acceleration of the cantilever deflection in the i^{th} measurement period, as given by

$$\bar{v}_k[i] = \frac{\bar{d}_k[i] - \bar{d}_k[i-1]}{t_k^i - t_k^{i-1}}, \quad \bar{a}_k[i] = \frac{\bar{v}_k[i] - \bar{v}_k[i-1]}{t_k^i - t_k^{i-1}} \quad (6)$$

Adaptive discrete nanomechanical mapping The POIdynamics index introduced above is then used to adaptively update the measurement sequence in each round of nanomechanical mapping (Step 2)—to assign measurement period to a POI in each round of mapping. Specifically, let $\mathbf{S}_I^p = \{1,2,\cdot,N_p\}$ be the set of the index of all POIs, and \mathbf{V}_i be the vector of the POI measured in the i^{th} mapping in the ascending order, i.e., $\mathbf{V}_i[j] \in \mathbf{S}^p$, $\mathbf{V}_i[1] \leq \mathbf{V}_i[2] \leq \cdots \leq \mathbf{V}_i[N_p]$, and $|\mathbf{S}^p| = |\mathbf{V}_i|$ (|S|: the cardinality of a finite set S, i.e., the number of elements in S). Thus, the adaptive planning is to determine the element of \mathbf{V}_i in each round of mapping. Specifically, in any given i^{th} round of mapping, if the i^{th} averaged acceleration, i.e., the time-curvature of the cantilever deflection, is below the threshold value at any given k^{th} POI, then its corresponding measurement will be released from the k^{th} POI and assigned to the POI of the maximum POI-dynamics index, i.e.,

$$\hat{\mathbf{V}}_{i}[k] = \begin{cases} \ell^{*}[i] & \text{if } \bar{a}_{k}[i] \leq \varepsilon_{i}, \\ \mathbf{V}_{i-1}[k] & \text{otherwise;} \end{cases}$$
 (7)

where $\ell^*[i] \in \mathbf{S}^p$ is the index of the POI with the maximum POI-dynamics index in the i^{th} round of mapping, i.e., $\bar{\phi}_{\ell^*[i],Dyn}[i] = \max_{1 \leq k \leq N_p} |\bar{\phi}_{k,Dyn}[i]|$, and ε_i is the threshold of the curvature in the i^{th} round of mapping

$$\varepsilon_i = \phi_{i,Dyn}^{\min} + \delta \left(\bar{\bar{\phi}}_{i,Dyn} - \bar{\phi}_{i,Dyn}^{\min} \right),$$
 (8)

where $\phi_{i,Dyn}^{\min}$ and $\bar{\phi}_{i,Dyn}$ are the minimum value and the mean value of the POI-dynamics index in the i^{th} round of mapping, respectively, and δ is the weight.

The i^{th} mapping sequence $\mathbf{V}_i[\cdot]$ will then be obtained by rearranging the elements in the above updated mapping sequence $\hat{\mathbf{V}}_i[\cdot]$ in the ascending order, $\hat{\mathbf{V}}_i[\cdot] \to \mathbf{V}_i[\cdot]$. Initially, a sequential mapping sequence will be followed in the first \mathbf{m}_0 rounds of mapping (e.g., $\mathbf{m}_0 = 3$) to obtain enough number of measurements at each POI for estimating the corresponding averaged velocity and acceleration, i.e., $\mathbf{V}_i[\cdot] = \mathbf{V}_0[\cdot]$ for $i = 1, 2, \dots, \mathbf{m}_0$.

Moreover, to avoid that the measurement is overly concentrated to the POI of the maximum dynamics variation, or the dynamic variation at other POIs is missed, a reset mechanism is utilized to reinforce the measurement on all the POIs via sequential mapping sequence. Specifically, the original sequential mapping, $\mathbf{V}_0[\cdot]$ will be restored when (1) the number of successively repetitive measurements at a POI exceeds the threshold number $\mathbf{m}_{r,1}$, or (2) the number of distinct POIs measured in one round of mapping is less than the threshold value $\mathbf{m}_{r,2}$, i.e.,

$$\mathbf{V}_{i}[j] = \mathbf{V}_{0}[j], \quad \text{if}$$

$$\exists \mathbf{k}_{r}, \text{ such that } \mathbf{V}_{s}[\mathbf{k}_{r}] = \mathbf{V}_{i}[\mathbf{k}_{r}],$$

$$\text{for } s = i - 1, i - 2, \cdots, i - \mathbf{m}_{r,1} + 1,$$

$$\text{or } |\mathbf{V}_{i}| \leq \mathbf{m}_{r,2}$$

$$(9)$$

where $\mathbf{V}_{i,\mathrm{dist}}$ denotes the vector of POIs in the i^{th} round of mapping with the repeated POIs removed.

3. EXPERIMENTAL DEMONSTRATION

The proposed A-DNM technique was illustrated through experiments conducted on a PHBV polymer sample undergoing crystallization process.

3.1 Experimental setup

The experiments were conducted on a commercial AFM (Dimension Icon, Bruker Inc.) on which all the piezo actuators, sensors, and cantilever deflection signals in three dimensions can be directly accessed. All of the signals were acquired through a computer-based data acquisition system (NI-6259, National Instruments Inc.) under the Matlab xPC-target (Mathworks, Inc.) environment. A cantilever probe (model: RFESP-75) with spring constant of 3 N/m was used.

A PHBV polymer undergoing liquid-to-solid phase transition was measured. The crystal nucleation from the liquid state exhibits heterogeneous dynamic nanomechanical properties in both spatial and temporal domains, serving well to validate the efficacy and efficiency of the A-DNM compared to the DNM. The proposed ADNM was validated during the forming process of the circular spherulite when the PHBV polymer was cooling to 22°C and fully crystallized, as shown in figure 2. This melting-cooling process was repeated in the experiments.

3.2 Implementation of the A-DNM on the PHBV Polymer undergoing Crystallization Process

First, in the initialization step (Step 0), first the optimal control inputs for rapid probe engagement and withdrawal were obtained on the crystalized PHBV sample, as described in Wang and Zou (2020). A total of 12 POIs were prescribed across a large area of the PHBV polymer. Second, rapid probe engagement and withdrawal and rapid nanomechanical measurement at the chosen POIs were obtained by following the steps in the proposed technique, as described in Section 2. Finally, the proposed online adaptive mapping of the measurement sequence was implemented, where the POI-dynamics index was calculated was calculated by using the averaged probe force (i.e., cantilever deflection) and the averaged velocity and averaged acceleration of the force measured in the first three rounds of mapping via sequential mapping, and the reset to sequential mapping sequence was applied when the measurement on a POI was successively repeated for more than six times.

A total of ~ 1274 iterative measurements at each POI were acquired for 1100s to monitor the time-varying nanome-chanical property during the crystallization process. The elastic modulus E was quantified by using the control-based nanomechanical measurement technique Wang and Zou (2020), where the excitation force on the material was tracked using the MIIC technique on a hard reference sample, and the indentation generated on the PHBV sample $\Delta_z(t)$ was quantified as the difference between the cantilever base displacement on the soft polymer sample, $z_{bs}(t)$, and that on the hard sample, $z_{bh}(t)$, $\Delta_z(t) = z_{bs}(t) - z_{bh}(t)$, and the elastic modulus of the PHBV sample can be obtained via the Hertzian contact model Ren et al. (2013) with the applied force:

$$F_z=\frac{4}{3}\frac{E\sqrt{R\Delta_z^3}}{1-\nu^2} \eqno(10)$$
 with the tip radius $R=8nm,$ and the Poisson ratio of the

with the tip radius R=8nm, and the Poisson ratio of the polymer $\nu=0.5$. The dynamic elastic moduli at the 12 POIs measured via the A-DNM are shown in figure 3.

3.3 Discussion

First, the experimental results showed that the effect of the time-varying sample height (during the liquid-solid phase transition of the PHBV sample) on the mapping (Objective \mathcal{O}_1) was accounted for. The desired preload force was reached in all POIs during the entire mapping process. Such a consistent probe engagement was obtained by reliably estimating the sample height at each POI, then accounting for it in the between-POI transition of the probe and the following rapid probe engagement process. The experimental results also demonstrated the efficacy of the proposed adaptive mapping sequence planning (Objective \mathcal{O}_2). Compared to the sequential R-DNM method, the proposed A-DNM can effectively capture the fast temporal variation of the elastic moduli of the PHBV polymer during the crystallization process. More measurements were acquired at the POI of the maximum POIdynamics index in each round of mapping. As shown in figure 3, the temporal resolution of the elastic moduli at POIs (a), (d), (f) were much higher than those at POIs (b), (c), (e) during the time when the curvature of the time-elasticity curve were much larger at POIs (a), (d), (f) than that at POIs (b), (c), (e), respectively. Then, reset of the sequential mapping in every 6 rounds of mapping allowed us to acquire the mechanical variations at those infrequently-visited POIs. Moreover, the experimental results also demonstrated the advantageous of the proposed A-DNM over the previous R-DNM in capturing the dvnamic nanomechanical evolution during the crystalization process. As shown in figures 3, by using the proposed adaptive planning, more measurements were acquired on the faster-varying POI (c) than other POI, as well as on rapid-slope regions at POI (h) and (l). Thus, the experimental results demonstrated that the proposed A-DNM was capable of planning the measurements adaptively to capture the nanomechanical evolutions during dynamic processes.

4. CONCLUSION

This paper proposed an approach to adaptively map time-varying nanomechanical properties of a soft sample undergoing dynamic evolution, through an extension of the recently-developed discrete nanomechanical mapping (DNM). First, the time-varying sample topography during the dynamic evolution was estimated by using the measured data, and then accounted for in the cantilever probe transition between the POIs and the following probe engagement at each POI. Secondly, a POI-dynamics index was proposed based on the measured cantilever deflection to quantify the relative speed of the nanomechanical evolution between the POIs, and then used to adaptively plan the measurement time between the POIs. The effectiveness and efficiency of the proposed ADNM technique was evaluated and validated through an AFM experiment on a poly(3-hydroxybutyrate-co-3-hydroxyvalerate) (PHBV) polymer undergoing the crystalization process, with comparison to the DNM method.

REFERENCES

Braker, R.A., Luo, Y., Pao, L.Y., and Andersson, S.B. (2018). Hardware demonstration of atomic force microscopy imaging via compressive sensing and μ -path

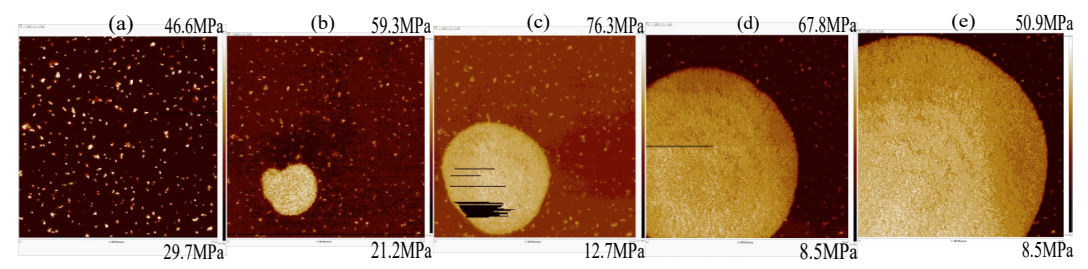


Fig. 2. The $10\times10~\mu m$ modulus images of the PHBV polymer sample after heating at 220 C° and cooling on the stage for (a) 50mins, (b) 58mins, (c) 1h6mins, (d) 1h18mins, (e) 1h35mins, respectively.

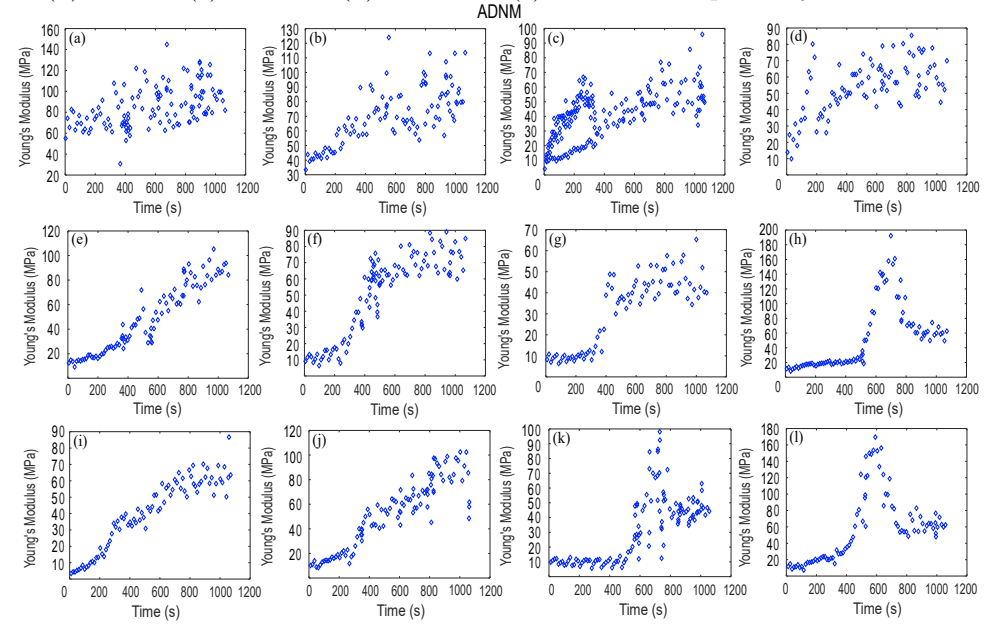


Fig. 3. (a-l) The dynamic Young's moduli evolution measured by using the A-DNM method at 12 prescribe locations during the PHBV polymer crystallization process.

scans. In 2018 Annual American Control Conference (ACC), 6037–6042. IEEE.

George, M., Nziakou, Y., Goerke, S., Genix, A.C., Bresson, B., Roux, S., Delacroix, H., Halary, J.L., and Ciccotti, M. (2018). In situ afm investigation of slow crack propagation mechanisms in a glassy polymer. *Journal* of the Mechanics and Physics of Solids, 112, 109–125.

Hobbs, J.K., Farrance, O.E., and Kailas, L. (2009). How atomic force microscopy has contributed to our understanding of polymer crystallization. *Polymer*, 50(18), 4281–4292.

Kim, K.S. and Zou, Q. (2013). A modeling-free inversion-based iterative feedforward control for precision output tracking of linear time-invariant systems. *IEEE/ASME Transactions on Mechatronics*, 18(6), 1767–1777.

Kodera, N., Noshiro, D., Dora, S.K., Mori, T., Habchi, J., Blocquel, D., Gruet, A., Dosnon, M., Salladini, E., Bignon, C., et al. (2021). Structural and dynamics analysis of intrinsically disordered proteins by highspeed atomic force microscopy. *Nature Nanotechnology*, 16(2), 181–189.

Pittenger, B., Slade, A., Berquand, A., Milani, P., Boudaoud, A., and Hamant, O. (2013). Toward quantitative nanomechanical measurements on live cells with peakforce qnm. doi:10.13140/RG.2.1.2163.2409.

Ren, J., Yu, S., Gao, N., and Zou, Q. (2013). Indentation quantification for in-liquid nanomechanical measurement of soft material using an atomic force microscope:

Rate-dependent elastic modulus of live cells. *Physical Review E*, 88(5), 052711.

Ren, J., Zou, Q., Li, B., and Lin, Z. (2014). High-speed atomic force microscope imaging: Adaptive multiloop mode. *Physical Review E*, 90(1), 012405.

Wang, J., Li, X., Zou, Q., Su, C., and Lin, N.S. (2020). Rapid broadband discrete nanomechanical mapping of soft samples on atomic force microscope. *Nanotechnology*, 31(33), 335705.

Wang, J. and Zou, Q. (2020). Rapid probe engagement and withdrawal with force minimization in atomic force microscopy: A learning-based online-searching approach. *IEEE/ASME Transactions on Mechatronics*, 25(2), 581–593.

Yan, B., Ren, J., Liu, Y., Huang, H., Zheng, X., and Zou, Q. (2017). Study of cholesterol repletion effect on nanomechanical properties of human umbilical vein endothelial cell via rapid broadband atomic force microscopy. *Journal of Biomechanical Engineering*, 139(3), 034501.